New Journal of Physics
The open access journal at the forefront of physics

Deutsche Physikalische Gesellschaft DPG IOP Institute of Physics

PAPER • OPEN ACCESS

Strain and electric field control of magnetism in $La_{(1-x)}Sr_xMnO_3$ thin films on ferroelectric $BaTiO_3$ substrates

New Journal of Physics
The open access journal at the forefront of physics

Deutsche Physikalische Gesellschaft DPG
IOP Institute of Physics

Published in partnership with: Deutsche Physikalische Gesellschaft and the Institute of Physics

OPEN ACCESS

RECEIVED
7 January 2020

REVISED
2 March 2020

ACCEPTED FOR PUBLICATION
23 March 2020

PUBLISHED
5 May 2020

PAPER

Strain and electric field control of magnetism in $La_{(1-x)}Sr_xMnO_3$ thin films on ferroelectric $BaTiO_3$ substrates

Markus Schmitz[1], **Alexander Weber**, **Oleg Petracic**, **Markus Waschk**, **Paul Zakalek**, **Stefan Mattauch**, **Alexandros Koutsioubas** and **Thomas Brückel**

Jülich Centre for Neutron Science JCNS and Peter Grünberg Institute PGI, JARA-FIT, Forschungszentrum Jülich GmbH, 52425, Jülich, Germany

[1] Author to whom any correspondence should be addressed.

E-mail: m.schmitz@fz-juelich.de

Keywords: magneto-electric, polarized neutron reflectometry, ferromagnetic, ferroelectric, strain-induced coupling, electric field control

Supplementary material for this article is available online

Abstract

We report on the observation of strain- and magneto-electric coupling in a system consisting of a thin film of ferromagnetic $La_{(1-x)}Sr_xMnO_3$ (LSMO, $x = 0.5$ and 0.3) on a ferroelectric $BaTiO_3$ (BTO) substrate. Pronounced magnetization steps occur at the BTO structural phase transitions. We associate these steps with a strain induced change of the magnetic anisotropy. Temperature dependent magneto-electric coupling could be evidenced by the magnetic response to an applied AC electric field in all ferroelectric phases of the BTO substrate. In a DC electric field, the magnetization changes are asymmetric with respect to the polarity. Polarized neutron reflectometry hints to oxygen migration as possible mechanism for this asymmetry. It also reveals strain-induced magnetization changes throughout most of the thickness of 252 Å ($x = 0.5$) and 360 Å ($x = 0.3$), respectively, of the LSMO layer. We conclude that the change of the magnetization depth profile at the interface as previously proposed by *ab initio* calculations is not the relevant mechanism. Instead strain, oxygen vacancies and frustration at interfacial steps dominate the magnetic response to an applied electric field.

1. Introduction

The understanding and manipulation of highly correlated electron systems in complex oxides is of great interest due to the large amount of possible applications [1]. Highly correlated electron systems, including in particular transition metal oxides, have a huge variety of unique properties [2], like superconductivity [3], colossal magnetoresistance [4], magnetocaloric effects [5], multiferroic effects [6], and many more [7]. The control of an ordering parameter with the conjugate field of a second different one, e.g. magneto-electric coupling [8], can lead to numerous applications, like magnetic field sensors and data storage devices with a four- or eight-state [9, 10] logic in a single device. For storage devices this can lead to combined advantages of FeRAMs and MRAMs, a non-volatile magnetic storage with bits switched by electric fields [11]. Thin films and material combinations with atomically flat interfaces can be produced [12, 13]. In those artificially fabricated heterostructures further interesting phenomena emerge due to finite size or coupling effects at interfaces [14, 15]. The combination of a strong ferromagnetic with a ferroelectric material can lead to an artificial multiferroic system via the coupling at the interface. A magneto-electric effect was reported in a $La_{0.8}Sr_{0.2}MnO_3/PbZr_{0.2}Ti_{0.8}O_3$ heterostructure [16], but a much more desired non-toxic, lead free system is of great interest due to ecological reasons. Strain and electric field control of magnetism in iron-oxide nanoparticle–BTO composites was reported by Wang *et al* [17]. Burton *et al* predict the control of magnetization by application of an electric field at the interface between $La_{0.5}Sr_{0.5}MnO_3$ and $BaTiO_3$ [18]. First-principle calculations suggest that a change in the electron density at the interface due to the reversal of the ferroelectric polarization of the $BaTiO_3$ leads to a change in the magnetic order at the interface from ferromagnetic to antiferromagnetic. The experimental verification of

this prediction is the motivation for our study. Recently, BTO/LSMO systems have attracted attention for multiple reasons like ferroelectric tunneling junctions [19, 20], magnetocaloric effects [21], magnetic anisotropy switching [22, 23], magneto-electric coupling [24], dielectric properties [25, 26] and electric field controlled magnetoresistance [27].

Here, heterostructures of LSMO and BTO are produced by oxide molecular beam epitaxy and high pressure oxygen sputtering. Control of magnetic properties is evidenced with a SQUID magnetometer, which was modified to allow for the application of electric fields and determination of the magnetoelectric coupling. Additionally, magnetic profiles are determined by polarized neutron reflectometry. Our results cannot be explained by the mechanism proposed by Burton *et al* as in real systems processes dominate that are not taken into account in the theory, such as oxygen migration or strain medicated coupling.

2. Sample properties

$BaTiO_3$ has four structural phases with a paraelectric cubic phase above 393 K. At lower temperatures it undergoes several ferroelectric first order phase transitions from cubic to tetragonal (Tet) (≈393 K), tetragonal to orthorhombic (Or) (≈278 K) and orthorhombic to rhombohedral (Rh) (≈183 K) [28]. $La_{(1-x)}Sr_xMnO_3$ has a rich magnetic phase diagram with respect to doping level and temperature [29]. Magnetic properties can be influenced e.g. by temperature or by strain [30, 31].

3. Sample preparation

$La_{0.53}Sr_{0.47}MnO_3$ LSMO[0.5] (252 Å) films have been grown on single crystalline (001) $BaTiO_3$ substrates (MaTeck, 0.5 mm thick) by a state of the art oxide molecular beam epitaxy system using Knudsen cells to evaporate the individual materials and an oxygen plasma source. The required growth rates were monitored by quartz micro balances under growth conditions. LSMO layers were grown by co-deposition at 900 °C with an oxygen flow of 0.1 sccm and a plasma power of 300 W. Rutherford backscattering RBS measurements confirm a stoichiometry of $La_{0.53}Sr_{0.47}MnO_3$ close to the transition from FM to AFM phase of LSMO [29]. *In situ* characterization with reflection high energy electron diffraction and low energy electron diffraction prove the crystalline structure with a low surface roughness of the prepared films. X-ray reflectometry measurements confirm a low surface roughness of 5.5 ± 0.1 Å. Additionally, $La_{0.7}Sr_{0.3}MnO_3$ LSMO[0.3] (360 Å) films have been grown on $BaTiO_3$ substrates by a high pressure oxygen sputtering system. The growth process was carried out at 900°C with an oxygen pressure of 3 mbar in order to achieve the exact stoichiometry certified by RBS measurements. For both samples an Au contact layer was deposited at the reverse side of the substrate for the application of electric fields.

4. Results and discussion

Magnetometry measurements were performed by a SQUID magnetometer (MPMS XL, Quantum Design). Figure 1 shows the temperature dependent magnetization for (a) LSMO[0.5] and (b) LSMO[0.3] with an applied in-plane magnetic field of $\mu_0 H = 10$ mT. Field-cooling (FC) and warming (FW) cycles were performed with a temperature rate of 2 K min^{-1}. The magnetization curves of both samples show a ferromagnetic shape for each structural phase of the BTO substrate with a T_C of 326 K and 310 K for LSMO[0.3] and LSMO[0.5], respectively. The reduced T_C compared to the bulk value can be explained by tensile in-plain strain since LSMO is grown as thin film [29, 32]. The out-of-plane lattice parameter c_{LSMO} = 3.85 Å for LSMO (see the supplementary data, available online at stacks.iop.org/NJP/22/053018/mmedia is smaller as the bulk value of 3.86 Å underlining the suggestion of tensile in-plane strain under the assumption of a constant unit cell volume and biaxial strain. The comparison of the lattice parameter to literature values suggests that our LSMO films are partially relaxed [33]. Sharp steps of the magnetization are observed at the structural phase transition temperatures of BTO, emphasized by gray boxes. This change of the magnetization is forced by the abrupt change of the BTO lattice parameter in the first order phase transition. A temperature hysteresis effect of those magnetization steps is observed following the structural phase transitions of BTO emphasizing the relation to lattice distortions. Similar behavior could be found for Fe on BTO substrates [34–36]. As shown by the inset the magnetization steps decrease with increasing magnetic field but do not vanish in saturation field of 15 mT. For details of the evolution of epitaxial strain with temperature we refer to the supplement.

We associate the observed steps in the magnetization with the change of the magnetic anisotropy due to the strain-induced change of the local environment of the Mn atoms. It was shown that LSMO films on cubic substrates show biaxial magnetic anisotropy, while LSMO has uniaxial anisotropy on orthorhombic

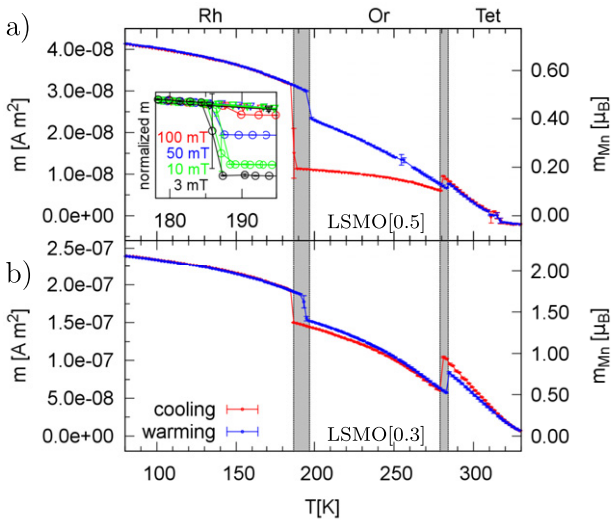

Figure 1. In-plane magnetization/magnetic moment vs temperature for (a) LSMO[0.5] and (b) LSMO[0.3] during FC and FW with a magnetic field of $\mu_0 H = 10$ mT. The inset shows the evolution of magnetization steps at the Or → Rh transition with respect to the external magnetic field. For a better visibility, the magnetization is normalized at 180 K. The step at the phase transition does not vanish in saturation field.

Table 1. Magnetic hardness m_r/m_s as a quantitative measure of magnetic anisotropy.

$\text{Phase}_{\text{BTO}}$	LSMO[0.5]	LSMO[0.3]
Tet	0.56 ± 0.02	0.58 ± 0.01
Or	0.08 ± 0.02	0.22 ± 0.05
Rh	0.73 ± 0.04	0.81 ± 0.02

substrates [37]. Here, the different types of substrate symmetries lead to a change of the magnetic anisotropy of the LSMO from an biaxial anisotropy in the Tet phase to an uniaxial anisotropy in the Or phase, back to a biaxial anisotropy in the Rh phase of the substrate. The magnetic hardness (quotient of the residual magnetization m_r and the saturation magnetization m_s, see table 1) was evaluated from magnetic hysteresis loops (see the supplement) as a quantitative measure of magnetic anisotropy. It clearly indicates the change of the magnetic anisotropy of the LSMO layer for each phase of the BTO substrate. In addition, lattice distortions alter the exchange interaction in the LSMO layer independent of the external magnetic field. Previous studies show the sensitivity of the magnetic properties of LSMO to strain, resulting in a magnetic phase diagram as function of the doping level x and the in-plane lattice strain [30, 32]. Tensile strain leads to antiferromagnetic properties of $La_{1-x}Sr_xMnO_3$ with $d_{x^2-y^2}$ orbital ordering [30, 31, 38, 39] and thus to a reduction of the total magnetization in the LSMO film.

So far, the manipulation of the magnetization by strain was considered. Even more fascinating is the possibility to tune the magnetization by the application of electric fields. In order to probe a possible magneto-electric coupling (MEC), the SQUID magnetometer was modified following Borisov *et al* [40]. With this technique a magnetic signal $\Delta m_{E_{AC}}$ induced by an applied electric AC-field can be measured precisely using the advantage of high sensitivity due to a lock-in technique. Since the sample is not moved through the pick-up coils, the detected signal is purely caused by the change of the magnetic moment in the sample induced by the AC-field and thus proves the magneto-electric coupling.

Figure 2 shows the observed MEC signal for LSMO[0.5] and LSMO[0.3]. Data were taken with an AC-electric field of ± 3 kV cm^{-1} at $f = 1$ Hz, an external magnetic field of 3 mT, and a cooling rate of 2 K min^{-1}. A clear MEC signal can be observed for both stoichiometries in the entire temperature range. The magnetic response to the electric field differs for each structural phase of BTO, but is pronounced in proximity to the BTO phase transition temperatures, where ferroelectric domain mobility is increased due to multiple domain orientations. In general the MEC signal follows a quite similar behavior as the temperature dependent piezoelectric coefficient (d_{33}) [41] of BTO. As the piezoelectric coefficient quantifies the volume change of a piezoelectric material under the application of an electric field we conclude that the observed MEC is strain induced. Thus, certainly the change of the magnetization is related to the strain induced to the LSMO layer by application of the AC electric field. For LSMO[0.3] the sign of the MEC signal changes within the Or phase of BTO meaning a change of the sign of the magneto-electric coupling.

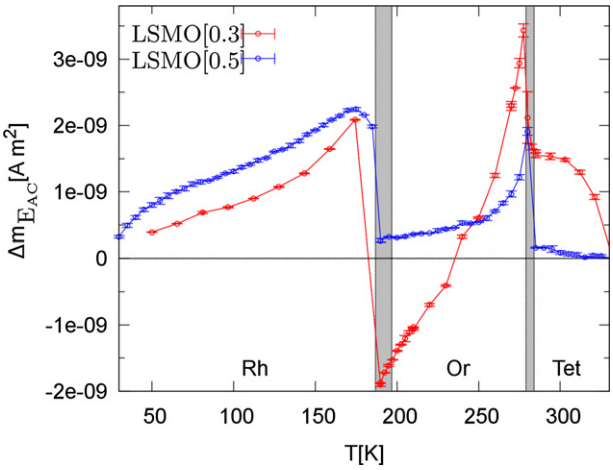

Figure 2. Magneto-electric coupling with respect to the applied AC electric field at $\mu_0 H = 3$ mT. MEC is pronounced at the phase transitions of the BTO substrate.

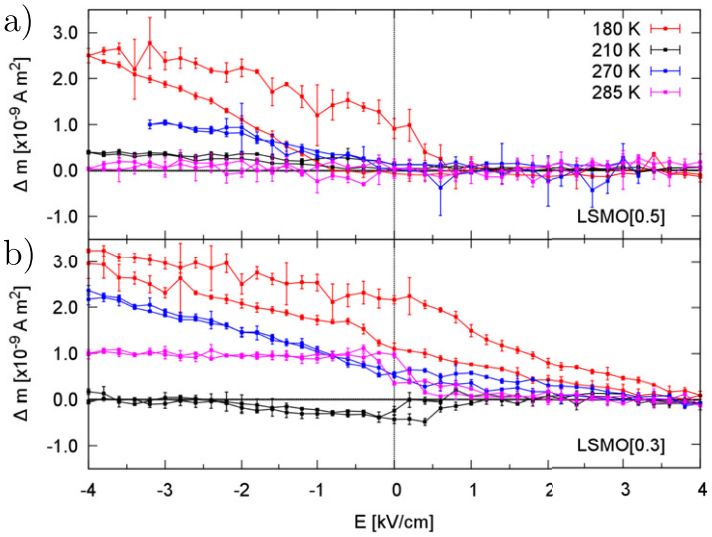

Figure 3. Modification of the magnetization Δm as function of applied DC electric field for (a) LSMO[0.5] and (b) LSMO[0.3] at various temperatures above and below the BTO phase transition temperatures.

For a more detailed view, DC electric field dependent magnetization measurements with a magnetic field of 3 mT were performed for both samples at temperatures above and below the BTO phase transitions. Samples were cooled down with a positive applied electric field of $+4$ kV cm^{-1}. Each electric loop ($+4$ kV cm^{-1} $\rightarrow -4$ kV cm^{-1} $\rightarrow +4$ kV cm^{-1}) was taken twice in order to eliminate artifacts due to domain formations related to the phase transitions. Here we only show the second measurement at each temperature. For a better comparability of the results at different temperatures, figure 3 shows the modification of the magnetization Δm compared to the magnetization at the starting point of the electric loop ($+4$ kV cm^{-1}) for (a) LSMO[0.5] and (b) LSMO[0.3].

One can clearly see an asymmetric change of the magnetization with respect to the polarity of the applied DC electric field. The change of the magnetization from positive to negative applied electric field nicely fits to the data taken with the newly implemented MEC technique (figure 2). For LSMO[0.3] the modification of the magnetization is negative at 210 K with negative applied electric field, which explains the reversal of the MEC signal in the Or phase.

5. Polarized neutron reflectometry

Polarized neutron reflectometry (PNR) was performed to deduce the magnetization profile of LSMO[0.5] at MARIA (MLZ) [42]. The magneto-electric coupling mechanism proposed by Burton *et al* [18] predicts a

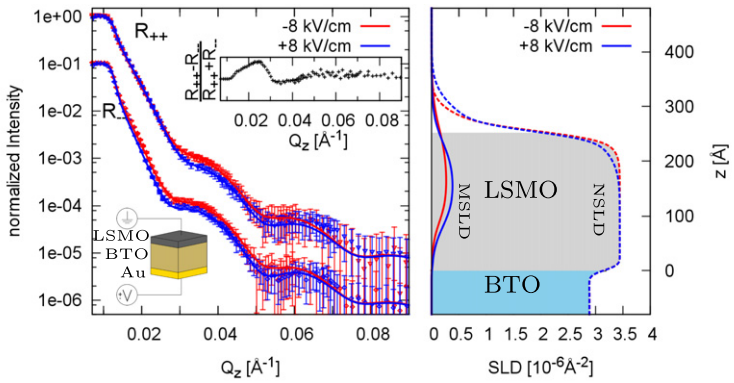

Figure 4. PNR data of LSMO[0.5] at 285 K with corresponding PNR fits (solid lines). R_{--} reflectivity is divided by 10 for a better visibility. Additionally, the SLD profiles obtained by the fits are depicted at the right side. The origin of the z-scale is at the LSMO/BTO interface.

change of magnetization in direct vicinity to the interface upon application of an electric field, which would show up in the PNR data. The temperatures are reached by cooling the sample in a magnetic field of 1 T. The measurement is performed in saturation, thus only non-spinflip channels are measured, R_{++} and R_{--} for neutron spin up and down, respectively, before and after the scattering process. The direction of the applied electric field is switched at the desired temperature. Figure 4 shows PNR data taken at 285 K for both stoichiometries including the corresponding fits for the reflectivities. For better visibility the R_{--} reflectivity is divided by a factor of 10. Additionally, the nuclear and magnetic scattering length densities (NSLD and MSLD) obtained by the fits are depicted on the right side as function of the sample thickness z. PNR data of LSMO[0.5] show thickness oscillations up to the third order. The spin-asymmetry $\left(\frac{R_{++}-R_{--}}{R_{++}+R_{--}}\right)$ plot (see inset) indicates a finite magnetization. A difference in the reflectivity for different electric field polarities is clearly observed. The fit of the PNR shown by the solid line nicely represents the data. The NSLDs resulting from the fits show a low roughness at the LSMO/BTO interface in the range of 1–2 unit cells. A top layer with reduced NSLD has to be taken into account. In case of positive applied electric field, an enlarged surface roughness was found leading to an earlier drop in the NSLD at the surface. The magnetic profile represented by the magnetic scattering length density shows a reduced magnetization at the LSMO/BTO interface which can be explained by strain, since tensile strain leads to an antiferromagnetic ground state in $La_{0.5}Sr_{0.5}MnO_3$ [30, 31]. A maximal magnetization of $0.8^{+0.1}_{-0.1}$ μ_B/Mn is obtained for positive electric field. $0.6^{+0.1}_{-0.2}$ μ_B/Mn is obtained for negative electric field. The reduction of the magnetization for negative applied electric fields is present within the whole sample, but not limited to the LSMO/BTO interface.

In total, the magnetization profile with respect to the electric field direction just slightly changes as can be seen in the MSLD, but again this effect is not limited to the LSMO/BTO interface.

Overall, a difference in the PNR data with respect to the applied voltage could be observed. A reduction of the NSLD for positive applied electric field was found at the surface. We assume that this can be related to an oxygen deficient top layer, since the application of an electric field can lead to the diffusion of oxygen ions. Electric field dependent differences in the magnetization profiles could be observed, but are not limited to the LSMO/BTO interface.

6. Summary and conclusion

The magnetization of the LSMO layer on a BTO substrate exhibits pronounced steps at the BTO structural phase transitions. We relate this observations to strain effects leading to a change in the magnetic anisotropy and the exchange interaction of the LSMO layer induced by the BTO substrate. Using partially complementary methods such as angle-dependent magnetization, x-ray absorption spectroscopy and transport measurements, Panchal *et al* [22] concluded that strain is the decisive factor controlling magnetic anisotropy switching. Our detailed studies on the magneto-electric coupling and the depth resolved magnetization profile obtained by polarized neutron reflectometry support their conclusion and give additional insight into the microscopic mechanism of the observed effects. Using a modified SQUID magnetometer, magneto-electric coupling could be evidenced by the magnetic response to an AC and DC electric field applied to the LSMO/BTO structures. The magnetic response is asymmetric with respect to the polarity of the DC electric field. In the Rh phase the system shows a 'switching behavior' known from

memory devices, i.e. the magnetization for vanishing electric field has different values for different E-field histories. Polarized neutron reflectivity elucidate the mechanism behind this unusual magneto-electric behavior. We take changes of the nuclear scattering length density close to the surface of the LSMO layer under inversion of the E-field polarity as indication for oxygen vacancy migration in the electric field, known e.g. from resistive switching metal-oxide/metal structures. Under inversion of the E-field polarity, the MSLD changes throughout a depth of more than 100 Å in the LSMO layer. No significant changes are visible at the interface between LSMO and BTO. These observations are inconsistent with the mechanism for magneto-electric coupling proposed by Burton *et al* [18], namely magnetic reconstructions at the LSMO/BTO interface induced by switching of electric polarization. The fact that no significant magnetization changes are observed at the interface and that both compositions show similar magneto-electric coupling (while the 'Burton-mechanism' should only work for the $x = 0.5$ sample) rule out this mechanism as the dominating effect for our system. The identification of strain effects in the temperature dependence of magnetization leads us to the conclusion that also the magneto-electric coupling is mainly strain-mediated in our systems.

To conclude, our experimental study shows the limitations of *ab initio* calculations of electronic structures at interfaces in explaining magneto-electric coupling effects in real systems. Real systems have a complexity which is not properly reflected in calculations assuming ideally flat interfaces and non-mobile atomic structures. Additional effects, not considered in these calculations can dominate. Namely there are e.g. frustration effects at the interfacial steps, oxygen vacancy migration under electric field or strain induced changes of magnetic anisotropy and exchange interactions. Combining MEC-effect measurements with depth resolved vector-magnetometry based on polarized neutron reflectometry can elucidate the complex mechanisms occurring in real systems.

ORCID iDs

Oleg Petracic https://orcid.org/0000-0002-5138-9832
Alexandros Koutsioubas https://orcid.org/0000-0001-9417-5108

References

[1] Heber J 2009 *Nature* **459** 28
[2] Tokura Y 1998 *Curr. Opin. Solid State Mater. Sci.* **3** 175
[3] Bednorz J and Müller K 1986 *Z. Phys.* B **64** 189
[4] Haghiri-Gosnet A-M and Renard J-P 2003 *J. Phys. D: Appl. Phys.* **36** R127
[5] Phan M-H and Yu S-C 2007 *J. Magn. Magn. Mater.* **308** 325
[6] Fiebig M 2005 *J. Phys. D: Appl. Phys.* **38** R123
[7] Izyumskaya N, Alivov Y and Morkoç H 2009 *Crit. Rev. Solid State Mater. Sci.* **34** 89
[8] Matsukura F, Tokura Y and Ohno H 2015 *Nat. Nanotechnol.* **10** 209
[9] Gajek M, Bibes M, Fusil S, Bouzehouane K, Fontcuberta J, Barthelemy A and Fert A 2007 *Nat. Mater.* **6** 296
[10] Yang F, Tang M H, Ye Z, Zhou Y C, Zheng X J, Tang J X, Zhang J J and He J 2007 *J. Appl. Phys.* **102** 044504
[11] Bibes M and Barthelemy A 2008 *Nat. Mater.* **7** 425
[12] Poppe U, Schubert J, Arons R, Evers W, Freiburg C, Reichert W, Schmidt K, Sybertz W and Urban K 1988 *Solid State Commun.* **66** 661
[13] Schlom D G, Chen L, Pan X, Schmehl A and Zurbuchen M A 2008 *J. Am. Ceram. Soc.* **91** 2429
[14] Hwang H Y, Iwasa Y, Kawasaki M, Keimer B, Nagaosa N and Tokura Y 2012 *Nat. Mater.* **11** 103
[15] Chakhalian J, Millis A J and Rondinelli J 2012 *Nat. Mater.* **11** 92
[16] Molegraaf H J A, Hoffman J, Vaz C A F, Gariglio S, van der Marel D, Ahn C H and Triscone J-M 2009 *Adv. Mater.* **21** 3470
[17] Wang L-M, Petracic O, Kentzinger E, Rücker U, Schmitz M, Wei X-K, Heggen M and Brückel T 2017 *Nanoscale* **9** 12957
[18] Burton J D and Tsymbal E Y 2009 *Phys. Rev.* B **80** 174406
[19] Gagarin A G, Tumarkin A V, Sapego E N, Kunkel' T S and Stozharov V M 2019 *Tech. Phys. Lett.* **45** 152
[20] Tumarkin A V, Gagarin A G, Odinets A A, Sapego E N and Kunkel T S 2019 *Ferroelectrics* **544** 49
[21] Giri S K, MacManus-Driscoll J L, Li W, Wu R, Nath T K and Maity T S 2019 *J. Phys. D: Appl. Phys.* **52** 165302
[22] Panchal G, Phase D M, Reddy V R and Choudhary R J 2018 *Phys. Rev.* B **98** 045417
[23] Gorige V, Swain A, Komatsu K, Itoh M and Taniyama T 2017 *Phys. Status Solidi* **11** 1700294
[24] Li T, Ma D, Li K and Hu Z 2018 *J. Alloys Compd.* **747** 558
[25] Wang J, Bai J, Luo B, Wang S, Jin K and Chen C 2018 *Acta Phys. Sin.* **67** 017701
[26] Li T, Wang H, Li K, Hu Z and Ma D 2017 *Mater. Res. Bull.* **94** 160
[27] Swain A, Komatsu K, Itoh M, Taniyama T and Gorige V 2018 *AIP Adv.* **8** 055808
[28] Cohen R E 1992 *Nature* **358** 136
[29] Hemberger J, Krimmel A, Kurz T, Krug von Nidda H-A, Ivanov V Y, Mukhin A A, Balbashov A M and Loidl A 2002 *Phys. Rev.* B **66** 094410
[30] Horiba K *et al* 2009 *Phys. Rev.* B **80** 132406
[31] Konishi Y, Fang Z, Izumi M, Manako T, Kasai M, Kuwahara H, Kawasaki M, Terakura K and Tokura Y 1999 *J. Phys. Soc. Japan* **68** 3790
[32] Tsui F, Smoak M C, Nath T K and Eom C B 2000 *Appl. Phys. Lett.* **76** 2421

[33] Lee M K, Nath T K, Eom C B, Smoak M C and Tsui F 2000 *Appl. Phys. Lett.* **77** 3547
[34] Venkataiah G, Shirahata Y, Itoh M and Taniyama T 2011 *Appl. Phys. Lett.* **99** 102506
[35] Brivio S, Petti D, Bertacco R and Cezar J C 2011 *Appl. Phys. Lett.* **98** 092505
[36] Sahoo S, Polisetty S, Duan C-G, Jaswal S S, Tsymbal E Y and Binek C 2007 *Phys. Rev.* B **76** 092108
[37] Boschker H, Mathews M, Houwman E P, Nishikawa H, Vailionis A, Koster G, Rijnders G and Blank D H A 2009 *Phys. Rev.* B **79** 214425
[38] Fang Z, Solovyev I V and Terakura K 2000 *Phys. Rev. Lett.* **84** 3169
[39] Schumacher D, Steffen A, Voigt J, Schubert J, Brückel T, Ambaye H and Lauter V 2013 *Phys. Rev.* B **88** 144427
[40] Borisov P, Hochstrat A, Shvartsman V V and Kleemann W 2007 *Rev. Sci. Instrum.* **78** 106105
[41] Park S-E, Wada S, Cross L E and Shrout T R 1999 *J. Appl. Phys.* **86** 2746
[42] Mattauch S *et al* 2018 *J. Appl. Crystallogr.* **51** 646